



# **Advanced Carbon Capture for steel industries integrated in CCUS Clusters**

#### **Innovation Action**

This project has received funding from the European Union's Horizon 2020 research and innovation programme under the Grant Agreement No 884418.

# D4.6 Report on "Numerical study of the impact of impure CO2 on storage in a depleted gas field in the North Sea" (Task 4.1.3)

Work Package: 4

Due date of deliverable: 31 March 2025
Actual submission date: 07 May 2025
Start date of project: 1 April 2020
The project duration: 60 months

Lead beneficiary for this deliverable: University College London

Contributors: Richard Porter, Sergey Martynov, Anindityo Patmonoaji

Dissemination level: Public (PU)



### **Table of Contents**

1.	Version log	3
2.	Definitions and abbreviations	4
3.	Executive summary	5
4.	Introduction	6
5.	Objectives	7
Tas	sk 4.1.3.1. Defining Input	7
Tas	sk 4.1.3.2. Basic Simulations	7
Tas	k 4.1.3.3. Realistic Simulations	7
Tas	k 4.1.3.4. Geotechnical evaluation of results	8
6.	Methodology and defining input	9
6.1	Defining input	<u>c</u>
6.2	Basic simulations	10
	6.2.1 Grid construction and reservoir model	10
	6.2.2 Initial conditions and fluid properties	11
	6.2.3 Well configuration and boundary conditions	11
	6.2.4 Simulation schedule	12
	6.2.5 Visualization and analysis	12
	6.2.6 Sensitivity analysis	12
6.3	Realistic simulations	13
6.4	Geotechnical evaluation of results	16
7.	Results	17
7.1	Basic simulation results	17
7.2	Realistic simulation results	26
8.	Discussion and geotechnical evaluation	33
9.	Summary and conclusions	35
10.	Bibliography / References	37



# 1. Version log

Version	Date	Released by Nature of Change	
1	6/5/2025	R.T.J. Porter	First version



# 2. Definitions and abbreviations

Abbreviations	Definitions		
EoS	Equation of State		
IPCC	Intergovernmental Panel on Climate Change		
IEA	International Energy Agency		
MATLAB	MATrix LABoratory		
MRST	MATLAB Reservoir Simulation Toolbox		
VE	Vertical Equilibrium		



#### 3. Executive summary

This report presents the findings of a comprehensive numerical study into  $CO_2$  storage in depleted gas reservoirs, addressing plume migration, pressure evolution, and geochemical interactions under both idealised and field-relevant conditions. Using the MATLAB Reservoir Simulation Toolbox (MRST), we first conducted a series of basic simulations in a homogeneous 3D reservoir. These confirmed fundamental behavior: a buoyant  $CO_2$  plume rising and spreading beneath caprock, pressure build-up near the injector that relaxes once injection ceases, and the onset of key trapping mechanisms such as structural entrapment under the seal, residual trapping in pore throats, and solubility trapping in brine.

Building on these insights, realistic simulations introduced geological heterogeneity representative of the P18-6 North Sea field, variable injection rates, and  $CO_2 - N_2$  mixtures. We found that higher background pressures confine lateral plume growth, while  $N_2$  dilution enhances buoyancy and increases plume footprint. A stepwise "ramp-up" injection schedule mitigates early overpressure compared to a constant-rate strategy, offering a simple operational lever to protect well integrity. Heterogeneity in porosity and permeability further modulates plume geometry, underscoring the need for detailed site characterisation.

To capture early geochemical feedback, a reactive-transport slice model tracked aqueous and mineral species over ten days of CO<sub>2</sub>-rich, low-salinity injection. Near the well, rapid acidification drives calcite dissolution, temporarily enhancing pore volume, while downstream zones show nascent re-precipitation that could gradually reduce permeability. These spatial patterns highlight where mineral trapping may emerge and where injectivity could evolve over time.

Finally, we synthesised pressure fields, saturation maps, and geochemical zoning into a preliminary geotechnical evaluation. This data-driven framework identifies the first two months of injection as the critical window for pressure management, confirms plume confinement within reservoir bounds, maps residual trapping footprints as early security against remobilisation, and forecasts zones of mineral alteration that may influence injectivity.

Collectively, these results deliver actionable guidance for CO<sub>2</sub> storage design: tailoring injection rates to reservoir pressure, anticipating plume extents based on fluid composition, and planning monitoring of both pressure and chemistry to safeguard seal integrity. While further work, particularly coupled geomechanical and long-term reactive-transport modelling, would deepen these insights, our study lays a clear methodological and interpretive foundation for the safe, efficient deployment of geological CO<sub>2</sub> storage.



#### 4. Introduction

Carbon Capture, Utilisation and Storage is considered as a major group of technologies for mitigation of CO<sub>2</sub> emissions into the atmosphere from industrial installations during the industrial transition to more sustainable means of production in the next decades. In particular, the EU has set plans for industrial decarbonisation, aiming to cut the industrial CO<sub>2</sub> emissions by at least 40% by the year 2030, compared to 1990 emissions levels, and become climate-neutral by 2050 [1]. As part of the Horizon 2020 programme on 'Low Carbon Industrial Production using CCUS', the C<sup>4</sup>U research project is aimed at making a significant step towards the development of highly efficient sorbent based technologies for CO<sub>2</sub> capture from iron and steel industries and demonstrating how these technologies can be implemented in industries in a most economically and environmentally sustainable manner.

Geological CO<sub>2</sub> storage is a key strategy in achieving global decarbonisation goals, with an estimated global storage capacity of approximately 1,000 gigatons (GtCO<sub>2</sub>), sufficient to accommodate emissions through to the end of the century [2]. The International Energy Agency (IEA) emphasises that without widespread CO<sub>2</sub> storage, global decarbonisation could become significantly more expensive [3]. CO<sub>2</sub> storage in geological formations, particularly depleted oil and gas reservoirs and saline aquifers, offers a viable solution for long-term carbon sequestration. However, challenges arise when transitioning from hydrocarbon extraction to CO<sub>2</sub> storage, especially around wellbores, where temperature and pressure differences can compromise the integrity of well seals [4].

The quality of the  $CO_2$  stream injected into geological formations plays a critical role in its behaviour and long-term stability. Impurities such as  $N_2$  and  $SO_2$ , commonly present in industrial  $CO_2$  streams, can influence the migration dynamics of  $CO_2$  plumes and alter the geochemical environment of the storage site.  $SO_2$  impurities, for instance, can increase the acidity of the formation brine, potentially leading to mineral dissolution and altering reservoir properties like porosity and permeability [5]. On the other hand,  $N_2$  reduces the density of  $CO_2$ , which may impact the  $CO_2$  plume's migration and increase the pressure required for injection, making it essential to study varying impurity concentrations in more detail.

Deliverable D4.6: Numerical study of the impact of impure CO<sub>2</sub> on storage in a depleted gas field in the North Sea contributes to the broader C<sup>4</sup>U project by investigating how CO<sub>2</sub> impurities, such as nitrogen (N<sub>2</sub>) affect the stability, plume migration, pressure dynamics, and long-term storage efficiency of CO<sub>2</sub> in geological reservoirs. As CO<sub>2</sub> storage plays an increasingly vital role in climate change mitigation, understanding these effects is essential for optimising storage design and ensuring safe and sustainable sequestration operations.

The MATLAB Reservoir Simulation Toolbox (MRST) [6] [7] is central to this work, providing the necessary pl

atform to develop and validate numerical models for simulating CO<sub>2</sub> plume migration and geochemical processes. MRST's flexible framework for coupled multiphase flow and geochemical processes makes it well-suited for simulating the effects of impurities on CO<sub>2</sub> storage performance. The toolbox enables the creation of grid geometries with realistic features such as heterogeneity that enhance the accuracy of the simulations, facilitating a detailed assessment of the long-term behaviour of CO<sub>2</sub> in a depleted gas field under varying injection scenarios.



Through the use of MRST, this deliverable provides an understanding of how CO<sub>2</sub> impurities affect geological storage sites and contributes to the development of optimised injection strategies and management practices that ensure the safe, efficient, and long-term containment of CO<sub>2</sub>.

#### 5. Objectives

The goal of Task 4.1.3 in the  $C^4U$  project is to assess the impact of  $CO_2$  streams of different quality injected into the geological formation for permanent storage, on geochemical reactions and associated alteration of formation fluids and rocks using computational models. This task uses the MRST platform to simulate  $CO_2$  plume migration and changes in reservoir characteristics. The objectives are structured to ensure comprehensive modelling, including defining input parameters, performing basic and realistic simulations, and evaluating long-term geotechnical outcomes.

#### Task 4.1.3.1. Defining Input

This task involves defining input parameters for the simulations using literature and prior studies. The specific objectives are:

- **Identification of secondary minerals:** Identify minerals in the Dutch North Sea storage site likely to interact with CO<sub>2</sub>, based on similar reservoirs and CO<sub>2</sub> impacts.
- Geophysical and geological parameters: Compile site-specific parameters (e.g., pressure, temperature, porosity, permeability) from target reservoirs for use in simulations.
- MRST configuration and EoS selection: Configure MRST to model the geological site
  accurately, selecting appropriate Equations of State (EoS) for CO<sub>2</sub> phase behaviour and
  mineral-fluid interactions

#### Task 4.1.3.2. Basic Simulations

This task conducts basic CO<sub>2</sub> injection simulations to verify the modelling approach and setup and define injection strategies. The specific objectives are:

- **Model setup verification:** Verify MRST model configuration for representation of geological and geophysical conditions.
- **Injection scenarios:** Simulate simplified CO<sub>2</sub> injection scenarios to define key parameters like injection rate and reservoir distribution.
- MRST simulation and benchmarking: Perform simulations focusing on fluid flow, pressure evolution, and CO<sub>2</sub> migration.

#### Task 4.1.3.3. Realistic Simulations

This task simulates complex CO<sub>2</sub> injection scenarios to evaluate realistic impacts on CO<sub>2</sub> plume migration, geochemical processes, and geological storage. The specific objectives are:

• CO<sub>2</sub> plume migration in a heterogeneous reservoir: Simulate CO<sub>2</sub> plume evolution in a layered, field-analogue model to capture both lateral and vertical migration patterns.



- Effect of CO<sub>2</sub> stream composition: Investigate how varying impurity levels (e.g., N<sub>2</sub> dilution) influence the spread and dynamics of the CO<sub>2</sub> plume.
- Reservoir property sensitivity: Assess how changes in key geological properties (porosity, permeability) impact plume retention and distribution.
- **Injection strategy and pressure response:** Compare different injection schedules (e.g., constant vs. staged rates) to evaluate their effects on pressure evolution and plume behaviour.
- Reactive-transport and fluid chemistry: Model early geochemical interactions aqueous speciation, pH buffering, and mineral equilibria -to understand how CO<sub>2</sub>-rich fluids perturb reservoir chemistry.

#### Task 4.1.3.4. Geotechnical evaluation of results

This task focuses on evaluating the long-term geotechnical impacts of CO<sub>2</sub> injection, drawing on simulation outputs to assess storage-site stability. The specific objectives are:

- Pressure development: Assess the pressure evolution during injection and shut-in periods, identifying critical times when overpressure might pose risks to seal integrity and formation stability.
- CO<sub>2</sub> plume confinement: Investigate the lateral and vertical confinement of the CO<sub>2</sub> plume relative to the caprock, assessing how the plume behaves over time and whether it remains confined within the reservoir extent.
- **Mineral feedback and injectivity:** Evaluate geochemical processes such as dissolution and precipitation of minerals in the reservoir, assessing how these processes affect injectivity and long-term storage stability.
- **Geological heterogeneity and trapping mechanisms:** Assess the influence of geological heterogeneity, including capillary and solubility trapping, on the immobilisation of CO<sub>2</sub> and the overall security of the storage site.
- Long-term site stability: Investigate the impact of CO<sub>2</sub> injection on reservoir characteristics, including pressure, temperature, gas saturation, and mineralogy, over relevant timescales.



#### 6. Methodology and defining input

The methodology for this study is structured to provide a systematic approach for evaluating the impact of CO<sub>2</sub> impurities on storage in a depleted gas field in the North Sea. The work involves defining key input parameters, performing basic and realistic simulations, and conducting a geotechnical evaluation of results to assess the long-term impacts of CO<sub>2</sub> injection. Each stage is designed to ensure accurate and reliable modelling of CO<sub>2</sub> plume migration, geochemical processes, and reservoir characteristics under varying conditions, ultimately contributing to the development of optimised storage strategies.

## 6.1 Defining input

The methodology for defining input parameters in Task 4.1.3.1 follows a structured approach to ensure accurate and site-specific data is incorporated into the MRST simulations. This process consists of three main steps: identification of secondary minerals, determination of geophysical and geological parameters, and the configuration of the MRST model with appropriate EoS. Each step is described below.

#### **Identification of secondary minerals**

The first step was to identify the secondary minerals likely to interact with CO<sub>2</sub> in the geological formation of the Dutch North Sea depleted gas field. This involved the following:

- **Literature review:** A thorough review of scientific literature and existing reports detailing the mineralogy of similar reservoirs and the interactions between CO<sub>2</sub> and minerals was conducted. Special attention is paid to studies that discuss CO<sub>2</sub>-induced geochemical reactions and mineral alterations in analogous depleted gas fields.
- **Data selection:** From the reviewed literature, relevant secondary minerals are identified based on their presence in applicable reservoirs and their potential to undergo dissolution or precipitation reactions when in the presence of CO<sub>2</sub>. These minerals were considered for inclusion in the geochemistry simulation model.

#### Determination of geophysical and geological parameters

Next, the necessary geophysical and geological parameters for the specific storage site were compiled. This was done by:

- **Data collection:** Data on reservoir characteristics such as pressure, temperature, porosity, permeability, and fluid composition were collected from available literature on the Dutch North Sea and other analogous sites.
- **Parameter validation:** The selected parameters were validated through comparison with similar geological formations in the region, ensuring that they reflected realistic conditions for the simulations. Any uncertainties were addressed through sensitivity analysis in realistic simulations, allowing for a range of input values to be considered.



#### MRST configuration and EoS selection

The third step was configuring the MRST model to accurately represent the reservoir conditions and CO<sub>2</sub> storage process. This includes:

- MRST setup: The MRST platform was configured to incorporate the site-specific parameters identified in the previous steps. This included defining the grid and geometry of the reservoir, setting initial conditions for pressure and temperature, and defining fluid properties.
- **EoS selection:** The most appropriate EoS was selected based on the expected CO<sub>2</sub> stream composition and the reservoir's geological characteristics. EoS models like the Peng-Robinson or Soave-Redlich-Kwong models were evaluated for their suitability to simulate the CO<sub>2</sub> phase behaviour and interactions with the formation fluids and minerals.
- **Input integration:** The selected secondary minerals and geophysical parameters were integrated into the MRST setup, ensuring that the input data was represented in a manner consistent with the expected CO<sub>2</sub> storage conditions and the site's geological characteristics.

#### 6.2 Basic simulations

The basic simulations were performed using the MRST along with several specialised modules, including **co2lab-common**, **co2lab-ve**, **ad-core**, **ad-props**, **ad-blackoil**, and **mrst-gui**. This open-source toolbox enables the modelling of two-phase flow in porous media and was adapted to simulate the behaviour of CO<sub>2</sub> in a depleted gas reservoir.

#### 6.2.1 Grid construction and reservoir model

A three-dimensional prism grid was generated to represent a section of a depleted CO<sub>2</sub> storage reservoir. The grid was constructed with the following features:

- Dimensions: The reservoir was defined by a top-surface depth of 1500 m, a full thickness
  of 100 m, and a lateral extent of 2000 m. A tensor grid was generated by defining
  coordinates that concentrate cells where greater detail was required.
- **Vertical resolution:** A total of 20 cells were used in the vertical direction (z) with cell thicknesses refined toward the top by employing a power law distribution.
- Lateral resolution: Approximately 25 cells in both the x and y directions were used, with increased resolution around the injection well (located at the bottom-centre cell).

While a dedicated grid dependence study was not performed, it is important to note that the chosen grid resolution affects the accuracy of the simulations. In particular, for the Vertical Equilibrium (VE) solution, finer grids typically lead to results closer to the full 3D solution, although this increases computation time. The results presented in this report are based on a specific grid resolution, with the understanding that further refinement may improve accuracy, particularly in areas with significant pressure gradients or flux variations.



Rock properties were uniformly assigned with a porosity of 0.25, selected for the initial scoping simulations to represent a high porosity sandstone consistent with values reported in the literature [8], and a permeability of 250 mD, within the range found in Dutch North Sea reservoirs [9]. These values provide a simplified yet representative model of the reservoir's heterogeneity.

#### 6.2.2 Initial conditions and fluid properties

The reservoir was initially saturated with brine, and the pressure field was set to a uniform, depleted state. For example, in the nominal primary simulation, a pressure value corresponding to 50 bar was set throughout the grid; alternative sensitivity analyses were performed by adjusting the initial pressure between 20 and 200 bar.

The CO<sub>2</sub> and brine fluids were modelled using MRST's initSimpleADIFluid function. Fluid properties were specified by:

- CO<sub>2</sub> properties: Density, viscosity, and compressibility were computed using tabulated data from the CO2props() function. A reference pressure (e.g., nominally 50 bar and adjusted to correspond with initial reservoir pressure sensitivity analysis) and temperature (70°C) were used for these calculations.
- **Brine properties:** The density was set at 1000 kg/m³ with near-zero compressibility to simplify the water phase behaviour and a fixed viscosity of 0.8 mPa·s.
- Rock compressibility was included at a representative value of 4.35 x 10<sup>-5</sup> bar<sup>-1</sup>.

Relative permeability and capillary pressure curves were adjusted to reflect hysteresis and interfacial effects:

- Relative permeability curves were modified using residual saturations of  $S_{rw}$ =0.27 and  $S_{rc}$ =0.20, implemented through custom expressions applied to the fluid.krW and fluid.krG fields.
- Capillary pressure was defined using a power-law function  $P_c(S_w)=P_eS_w^{-0.5}$  with entry pressure Pe=5 kPa.

All these parameters directly correspond to those defined in the MRST simulation script, which governs a two-phase (CO<sub>2</sub>–H<sub>2</sub>O) injection scenario over four years (two years post-injection).

#### 6.2.3 Well configuration and boundary conditions

A single injection well was defined in the bottom-centre cell of the grid. The well was configured to operate under a constant injection rate set to a predetermined value, i.e. 0.0682 m³/s, which corresponds to approximately 549 tonnes of CO<sub>2</sub> per day under nominal reservoir conditions (50 bar, 70°C). This rate was selected to represent a moderate-scale injection scenario suitable for field-scale modelling and sensitivity analysis.

Boundary conditions were imposed on all lateral faces of the grid. These were constructed by:



- Identifying faces that lie on the reservoir boundaries.
- Applying hydrostatic pressure conditions based on the neighbouring cell pressures. This ensured a realistic pressure gradient along the edges of the model.

#### 6.2.4 Simulation schedule

The simulation was divided into an injection phase of two years and a post-injection phase also of two years. Time step sizes were controlled via a ramp-up scheme to capture the early dynamics and then coarsened during the post-injection period. Two sets of control schedules were defined:

- **Injection period:** Active injection with a specified well rate.
- **Post-Injection period:** Wells were set to zero flow, allowing the model to simulate pressure dissipation and CO<sub>2</sub> plume migration.

The TwoPhaseWaterGasModel was used as the simulation model, handling the two-phase (CO<sub>2</sub>-brine) flow dynamics within the reservoir framework. The Automatic-Differentiation (AD) solver in MRST allowed for efficient computation over the defined time frame and grid.

#### 6.2.5 Visualization and analysis

The simulation results were analysed by extracting state variables (e.g., CO<sub>2</sub> saturation and pressure) at selected time steps. Multiple plotting strategies were employed, including:

- 1. **3D plots:** Time-lapse 3D visualisations were generated to show the evolution of the CO<sub>2</sub> plume. Cells with CO<sub>2</sub> saturation above 5% were highlighted in red.
- 2. **2D slices:** Cross-sectional views (both vertical and top-down) were produced by interpolating the data along specific slices (e.g., at x = 0) to observe detailed plume dynamics and pressure build-up.
- 3. **Line charts:** Lateral CO<sub>2</sub> spread in the top layer was analysed by binning CO<sub>2</sub> saturation data across x-coordinates and plotting the maximum values per bin. This provided insights into the lateral extent of CO<sub>2</sub> migration under varying initial conditions.
- 4. Trapping analysis using Vertical Equilibrium (VE) simulation: A VE analogue of the 3D model was implemented. A top-surface grid was derived to compute the trapping mechanisms (residual, solubility, structural, etc.) over time. The results were visualised as a stacked chart showing the evolution of different CO<sub>2</sub> trapping mechanisms during the injection and post-injection period.

#### 6.2.6 Sensitivity analysis

To examine the influence of initial reservoir pressure on CO<sub>2</sub> plume dynamics, a series of simulations were conducted for pressure values ranging from 20 to 200 bar. Each simulation produced datasets that were subsequently compared using both 3D and 2D visualizations, as well as quantitative analyses (e.g., lateral spread measurements). This multi-faceted approach provided a comprehensive understanding of how initial conditions influence plume migration, pressure buildup, and CO<sub>2</sub> trapping efficiency.



#### 6.3 Realistic simulations

To evaluate  $CO_2$  storage performance under field-relevant conditions, we conducted a suite of numerical experiments in MRST, progressing from a layered reservoir analogue to homogeneous flow-strategy tests and finally to a geochemically reactive 2D slice. All reservoir runs used MRST's compositional and two-phase solvers (with water treated explicitly as a distinct phase), while geochemical interactions were captured via the geochemistry toolbox.

#### 6.3.1 Reservoir analogue and model initialisation

Our principal model represents a depleted gas reservoir roughly analogous to P18-6 in the Dutch North Sea. A Cartesian grid spanning 1 km  $\times$  1 km horizontally and 100 m vertically was discretised into 30  $\times$  30  $\times$  10 cells. Five geological layers, with properties drawn from well logs and core data, were each mapped into two vertical cell layers (so that key heterogeneity is defined while small-scale textural noise is omitted). Table 1 summarises the base-case porosities and permeabilities.

Layer	Thickness (m)	Porosity	Permeability (mD)
Layer 1: Hardegsen 1	10	0.09	24
Layer 2: Hardegsen High Perm	10	0.20	550
Layer 3: Hardegsen 2	10	0.09	24
Layer 4: Upper Detfurth	35	0.075	12.6
Laver 5: Lower Detfurth	35	0.075	0.29

**Table 1:** Geophysical parameters for reservoir layers in the P18-6 field [9].

Initial reservoir states were generated with MRST's initCompositionalState, centring pressure at 52 bar and temperature at 387.45 K, with mole fractions of 50% water, 25% CO<sub>2</sub> and 25% hydrocarbons/impurities. The Peng–Robinson EOS (via NaturalVariablesCompositionalModel) provided fluid densities, viscosities, and phase behaviour, including binary interaction coefficients from Mallison et al. (SPE 79691) [10].

#### 6.3.2 Plume evolution under pure CO<sub>2</sub> injection

To establish a baseline, pure  $CO_2$  was injected at 0.0015 m³/s (1.5 L/s) from a single vertical injector in one corner of a quarter five-spot pattern. Injection continued for 2 years. Outputs were recorded at Day 33, 146, 365, and 730. At each of these times, we mapped the  $CO_2$  mole fraction throughout the reservoir and measured the plume's maximum lateral radius. These data underlie the time-series snapshots, as shown later in Figure 7.



#### 6.3.3 Effect of CO<sub>2</sub>/N<sub>2</sub> impurities

Following the pure  $CO_2$  runs, we repeated the same injection schedule (0.0015 m³/s for 2 years, then shut-in) using  $CO_2/N_2$  mixtures of 95%/5%, 80%/20%, and 50%/50%. All other model settings remained identical. Final plume footprints were extracted at Day 730 to produce the comparative plots in Figure 8.

#### 6.3.4 Sensitivity to porosity and permeability

Using the pure  $CO_2$  injection case (0.0015 m<sup>3</sup>/s), we conducted a parametric sweep in which each layer's porosity and permeability were simultaneously scaled by +10%, +20%, +30%, and +40%. Each variant was simulated over the same 2-year injection with outputs of  $CO_2$  saturation plotted in 3D at the final timestep.

#### 6.3.5 Injection strategy and pressure monitoring

To isolate operational effects from geology, we implemented two volume-equivalent injection schedules in a homogeneous reservoir (porosity = 0.075, permeability = 12.6 mD, representative of the Upper Detfurth Layer in far well area of the P18-6 field [9]):

- Constant-rate injection: 0.0015 m<sup>3</sup>/s continuously for 24 months, then 2 years of shut-in.
- Stepwise ramp-up injection:
  - Month 1: 0.0227 m<sup>3</sup>/s
     Month 2: 0.0455 m<sup>3</sup>/s
  - Months 3-24: 0.07125 m<sup>3</sup>/s
  - Months 25-48: Shut-in (0 m<sup>3</sup>/s)

These stepwise rates were chosen so that the cumulative CO<sub>2</sub> volume injected over 24 months exactly matches the constant-rate case. By ramping in three stages, we allow the reservoir to partially equilibrate before each increase, reducing early pressure spikes.

A single "monitoring" cell, located one layer immediately above the injector, was identified, and its pressure was temporally recorded. The resulting pressure-vs.-time curves (Figure 10) directly compare how the two strategies influence near-wellbore overpressure while delivering the same total CO<sub>2</sub> mass.

#### 6.3.6 Geochemical reactive transport

We ran a reactive-transport simulation on a  $20 \times 20 \times 1$  Cartesian slice using MRST's ChemicalTransportModel, coupling two-phase brine— $CO_2$  flow with full aqueous and mineral chemistry. The domain (porosity 0.5, permeability 1 D) was initially filled with high-salinity brine. A low-salinity,  $CO_2$ -rich fluid was injected at one boundary as one pore-volume per day, while opposed faces were held at 10 bar with zero-gradient outflow. These idealised parameters, particularly the high porosity and permeability, were selected to simplify flow behaviour and accelerate chemical equilibration in the domain, allowing clearer isolation of geochemical effects



rather than transport limitations. As such, they differ from those used in the field-scale simulations in Section 6.2, which focused on reservoir-scale heterogeneity and pressure dynamics.

In total, seventeen species were tracked:

- **Acid-base:** protons (H<sup>+</sup>) and hydroxide (OH<sup>-</sup>)
- Major ions: sodium (Na<sup>+</sup>), chloride (Cl<sup>-</sup>) and sodium hydroxide (NaOH)
- Solvent: water (H<sub>2</sub>O)
- Calcium system: free calcium (Ca<sup>2+</sup>), calcium bicarbonate (CaHCO<sub>3</sub>+), calcium hydroxide (CaOH+), aqueous calcium carbonate (CaCO<sub>3</sub>) and solid calcite (CaCO<sub>3</sub>(s))
- Carbonate system: carbonate (CO<sub>3</sub><sup>2-</sup>), bicarbonate (HCO<sub>3</sub><sup>-</sup>), aqueous CO<sub>2</sub> (CO<sub>2</sub>(aq)), gaseous CO<sub>2</sub> (CO<sub>2</sub>(g)), sodium bicarbonate (NaHCO<sub>3</sub>) and sodium carbonate (NaCO<sub>3</sub><sup>-</sup>)

Eleven equilibrium reactions were defined, including water dissociation, the full set of carbonate buffering steps, and calcite dissolution/precipitation. This acidification by dissolved CO<sub>2</sub> drives calcite dissolution near the well, and then allows re-precipitation where pH and ion concentrations recover downstream. The reaction set follows:

$$H_2O \rightleftharpoons H^+ + OH^-$$
 (1)

$$NaOH \rightleftharpoons Na^{+} + OH^{-}$$
 (2)

$$CaCO3(s) \rightleftharpoons CO3-2 + Ca+2$$
 (3)

$$CO_3^{-2} + H^+ \rightleftharpoons HCO_3^{-1} \tag{4}$$

$$CO_3^{-2} + 2H^+ \rightleftharpoons CO_2 + H_2O$$
 (5)

$$CO_2 \rightleftharpoons CO_2(q)$$
 (6)

$$Na^+ + HCO_3^- \rightleftharpoons NaHCO_3$$
 (7)

$$Na^{+} + CO_{3}^{-2} \rightleftharpoons NaCO_{3}^{-}$$
 (8)

$$Ca^{+2} + CO_3^{-2} + H^+ \rightleftharpoons CaHCO_3^{-1}$$
 (9)

$$Ca^{+2} + CO_3^{-2} \rightleftharpoons CaCO_3 \tag{10}$$

$$Ca^{+2} + H_2O \rightleftharpoons CaOH^+ + H^+ \tag{11}$$

We advanced the coupled flow–chemistry system for 10 days with adaptive time-stepping (five steps of 0.01 d, five of 0.1 d, then ten of 1 d). At days 0, 2, 4, 6, 8, and 10, we sampled concentrations of all seventeen species along the bottom row of cells (0–20 m) and plotted them on a logarithmic scale with distinct line styles and automatic colour cycling (Figure 11). This setup, explicitly including both aqueous and gas CO<sub>2</sub>, all relevant carbonate complexes, and solid calcite,



ensures reproducibility and fully captures the evolving acid front, carbonate speciation, and mineral feedback during early CO<sub>2</sub>-brine invasion.

#### 6.4 Geotechnical evaluation of results

In this phase, we translate our existing simulation outputs, pressure fields, CO<sub>2</sub>-saturation maps, and geochemical zoning, into a workflow for assessing storage-site stability.

We begin by extracting the full three-dimensional pressure fields at Days 33, 146, 365, and 730 from both the heterogeneous reservoir runs and the homogeneous injection-strategy cases. These snapshots, together with the time series from our dedicated "monitoring" cell, are plotted to reveal the build-up and relaxation of overpressure throughout the injection and shut-in periods.

Next, we overlay the CO<sub>2</sub> saturation contours at the same timesteps onto the reservoir grid in cross-section and plan views. By tracing the plume boundaries relative to the caprock interval, we confirm whether the plume remains confined under anticipated seal depths and identify the moment when lateral growth begins to taper off.

For geochemical feedback, the 20×1×1 reactive slice outputs at Days 0, 2, 4, 6, 8, and 10 are processed to compute the saturation index of calcite in each cell. Cells are categorized as dissolution-dominated, precipitation-dominated, or buffered, and these classes are mapped back onto the slice to highlight where mineral alteration might enhance injectivity or contribute to natural self-sealing.

Finally, we assemble these diagnostics, pressure evolution curves, plume-extent timelines, and mineral-stability zoning, into a suite of metrics that can be calculated using MRST outputs. This methodology provides a clear, data-driven basis for preliminary geotechnical conclusions on seal integrity, plume confinement, and mineral feedback over reservoir-relevant timescales, directly supporting the discussion and recommendations. Taken together, these analyses provide early indicators of conditions relevant to environmental safety, such as overpressure hotspots, plume confinement behaviour, and zones where mineral feedbacks may support long-term containment.



#### 7. Results

This section presents the results of simulations examining the impact of reservoir properties,  $N_2$  impurities, and geochemical interactions on  $CO_2$  injection into depleted gas reservoirs. The study focuses on how variations in porosity, permeability, and  $N_2$  concentration affect plume migration, reservoir pressure,  $CO_2$  saturation, and geochemical stability, with the aim of optimising injection strategies and assessing storage efficiency in heterogeneous formations. Initial baseline simulations were conducted to establish reference conditions, followed by more complex scenarios incorporating variable  $N_2$  levels, geological heterogeneity, and reactive transport processes. In addition to geotechnical analysis, geochemical simulations using the MRST framework were performed to investigate how  $CO_2$ -rich fluids perturb mineral equilibria and alter aqueous species distributions over time. These simulations capture key reactions such as dissolution, precipitation, and buffering dynamics that govern long-term chemical stability. The results highlight critical findings on plume behaviour, the influence of petrophysical properties, the diluting effect of  $N_2$  and the spatial-temporal evolution of chemical species under  $CO_2$  injection, with implications for storage integrity and reservoir performance.

#### 7.1 Basic simulation results

This section presents the results of basic simulations investigating  $CO_2$  injection and storage in a depleted gas reservoir. Using the MRST  $CO_2$ -lab module, the simulations explore key dynamics of  $CO_2$  migration, pressure evolution, and trapping mechanisms. Various initial reservoir pressures were considered to assess their impact on  $CO_2$  plume behaviour and storage efficiency. The findings provide a foundational understanding of the  $CO_2$  injection process, highlighting the roles of different trapping mechanisms, such as structural, residual, and solubility trapping. These results serve as a basis for more complex simulations aimed at improving  $CO_2$  storage capacity predictions over longer timescales.

The simulation output includes a series of visualisations that illustrate how  $CO_2$  behaves within the reservoir over time. One of the key figures, Figure 1, captures the expansion of the  $CO_2$  plume at several time intervals, ranging from six months to four years. These snapshots show the spatial distribution of  $CO_2$  as it migrates through the reservoir, highlighting the dynamic evolution of the plume as it responds to buoyancy and pressure gradients during and after 2 years of injection. At the initial reservoir pressure of 50 bar, the plume spreads to a radius of over 1500 m by the end of the 4-year simulation.

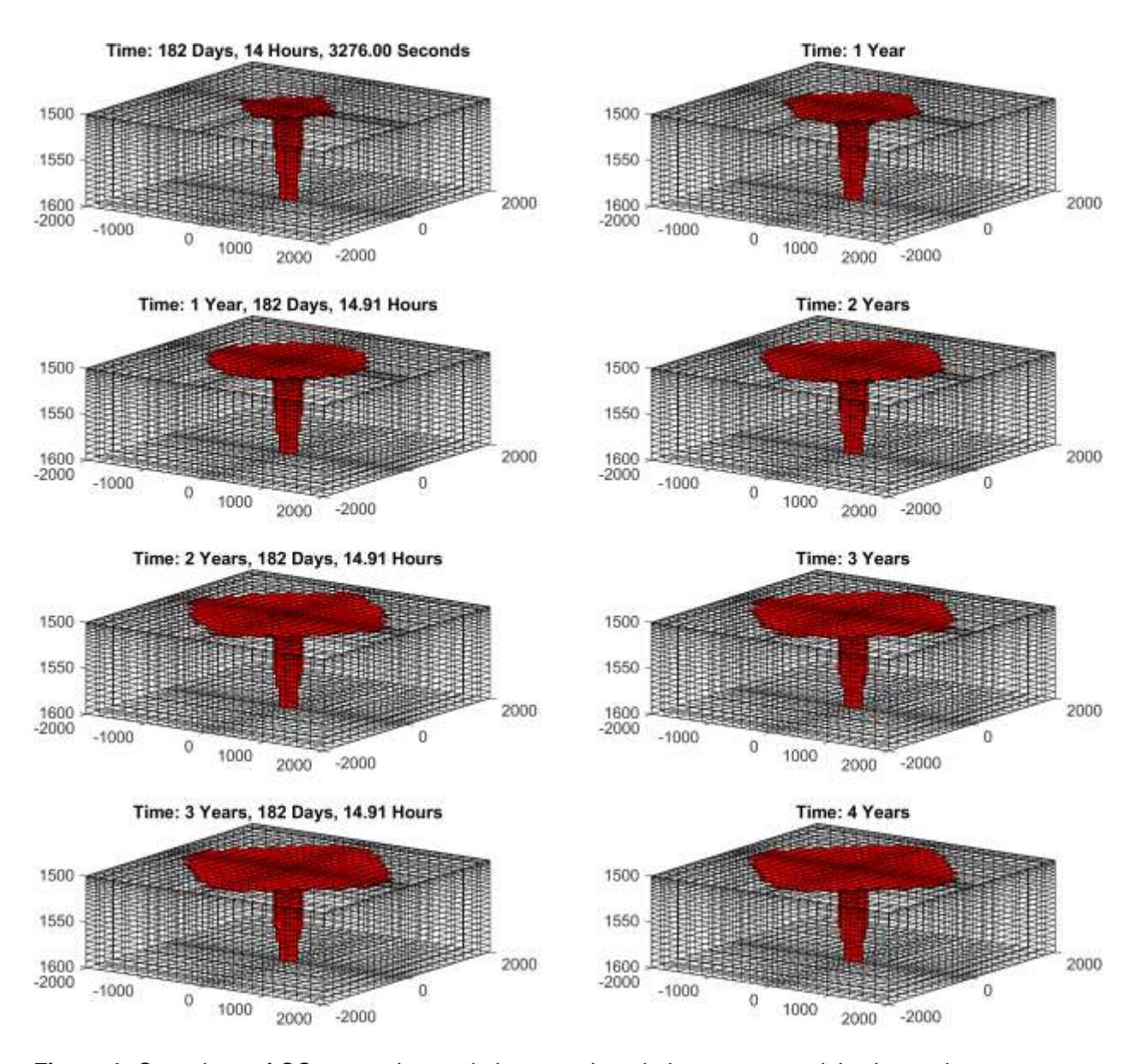


**Figure 1:** Snapshots of  $CO_2$  saturation evolution over time during a two-year injection and two-year post-injection period in a 50 bar reservoir system. Each subplot represents the  $CO_2$  saturation distribution at different time steps, with red indicating cells with  $CO_2$  saturation above 0.05, highlighting the movement and extent of the  $CO_2$  plume within the reservoir grid. The length scales are in meters.

Figure 2 provides a complementary perspective to Figure 1 via a vertical slice through the reservoir at approximately  $x \approx 0$ , showing how  $CO_2$  saturation evolves over time from six months to four years. This 2D visualisation complements the plan view in Figure 1 by revealing the vertical distribution of the  $CO_2$  plume within the reservoir. As the injection progresses, the plume rises buoyantly through the formation, forming a distinct saturation front. Even after injection stops, the plume continues to migrate upward due to buoyancy forces. A faint, light blue zone follows in the wake of the main plume body; this residual footprint indicates areas where  $CO_2$  is retained through



residual and solubility trapping. These regions are especially prominent along the upward migration pathway and illustrate the lasting impact of plume movement beyond active injection.

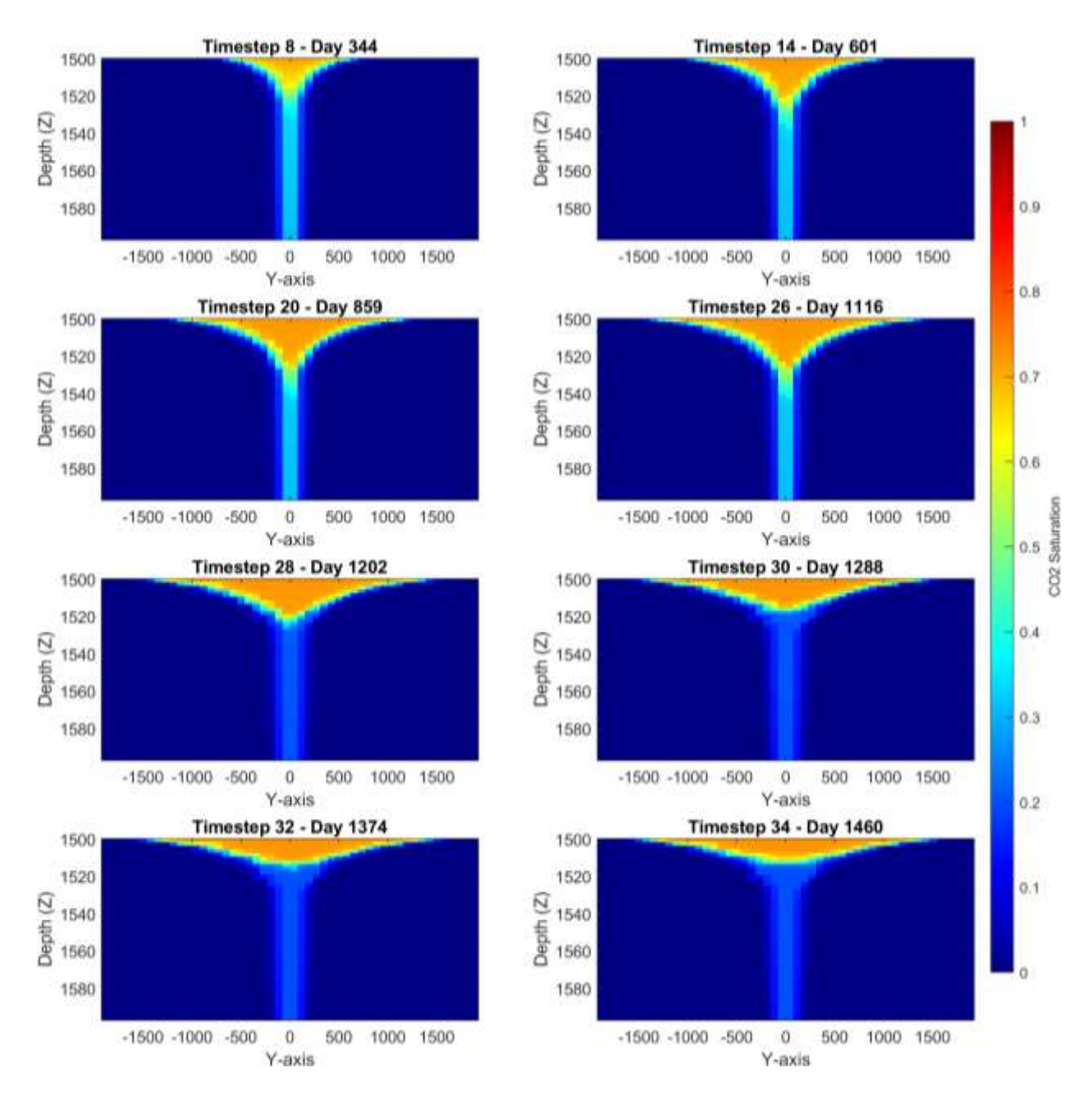


**Figure 2:** Evolution of  $CO_2$  saturation in a vertical slice (x  $\approx$  0) over time, illustrating the gravity-driven buoyant plume migration in the y-z plane. Each subplot corresponds to a different timestep, with  $CO_2$  saturation represented by the colour scale. Depth increases downward, and the time progression highlights plume development and upward migration due to buoyancy effects. The length scales are in meters.

Figure 3 shows a top-down view of the initial simulation, illustrating the horizontal evolution of CO<sub>2</sub> saturation across the reservoir over time. As the injection progresses, the plume gradually spreads outward from the injection point, with buoyancy driving lateral migration along the top of the formation. The colour scale highlights areas of higher CO<sub>2</sub> accumulation, showing how the plume flattens and extends over the four-year simulation. This visualisation complements the earlier figures by capturing the broader footprint of the plume and the influence of structural trapping on its containment.

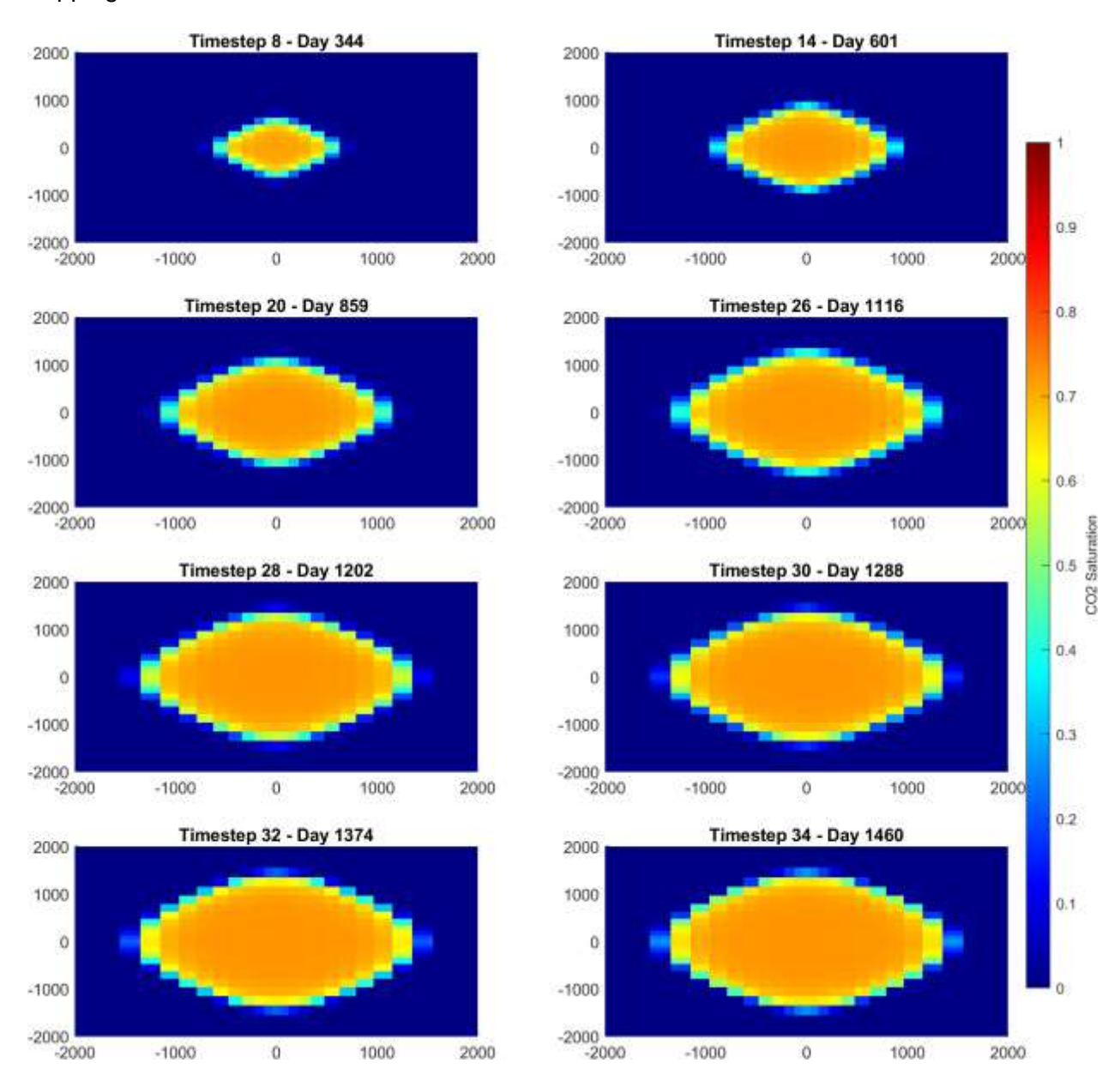


**Figure 3.** Top-down view of  $CO_2$  saturation evolution over time, showing the lateral migration and spreading of the buoyant plume at different timesteps. The colour scale represents  $CO_2$  saturation, with higher values indicating greater  $CO_2$  accumulation in the reservoir. The length scales are in meters.

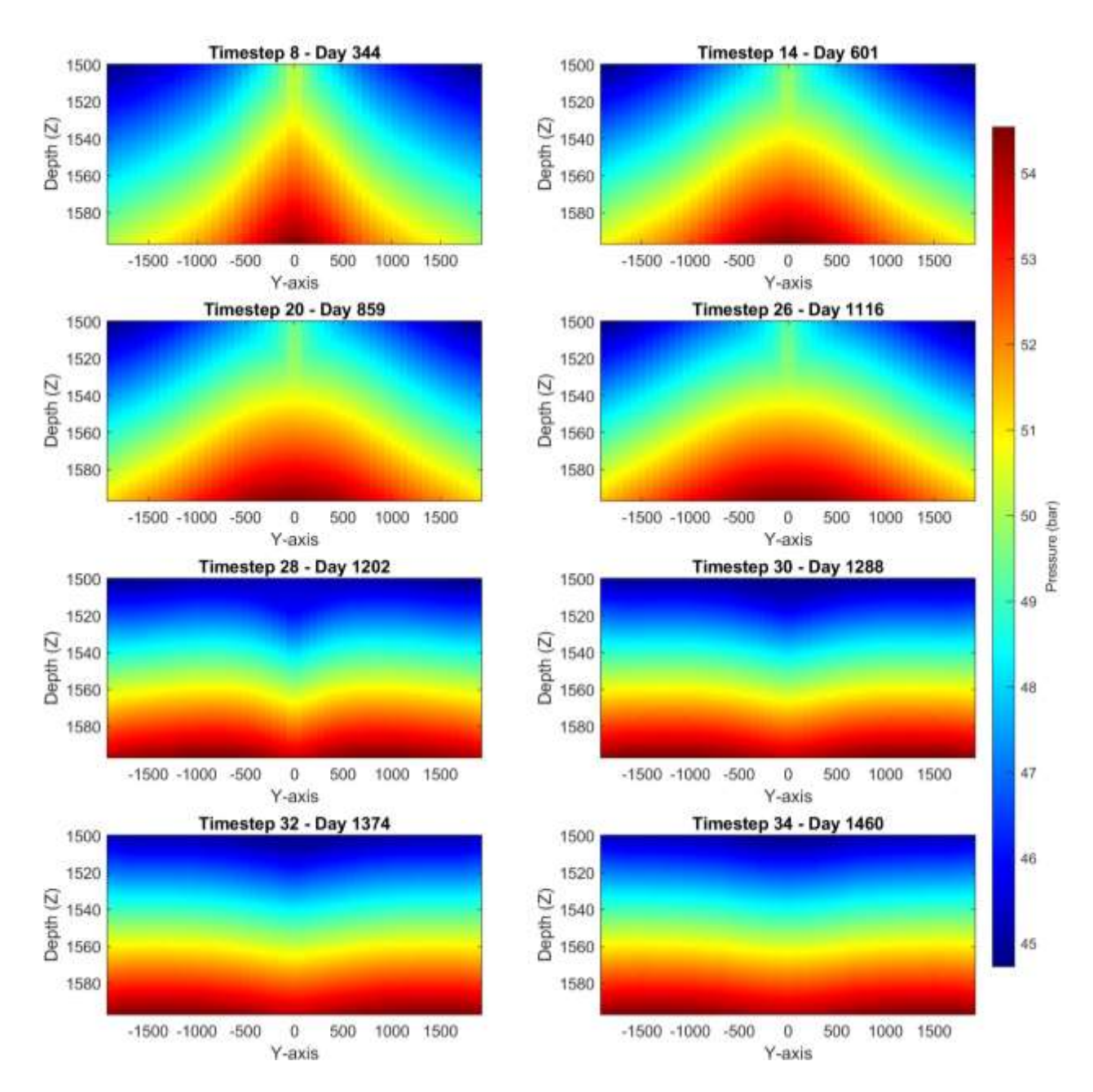


**Figure 4**: Evolution of pressure in a vertical slice ( $x \approx 0$ ) over time, illustrating the pressure distribution and its variation within the subsurface over the simulation period. Each subplot corresponds to a different timestep, with pressure represented by the colour scale. Depth increases downward, and the time progression highlights changes in pressure, showing both the build-up and dissipation of pressure as it evolves throughout the system, reflecting the dynamics of fluid migration and the system's response over time. The length scales are in meters.

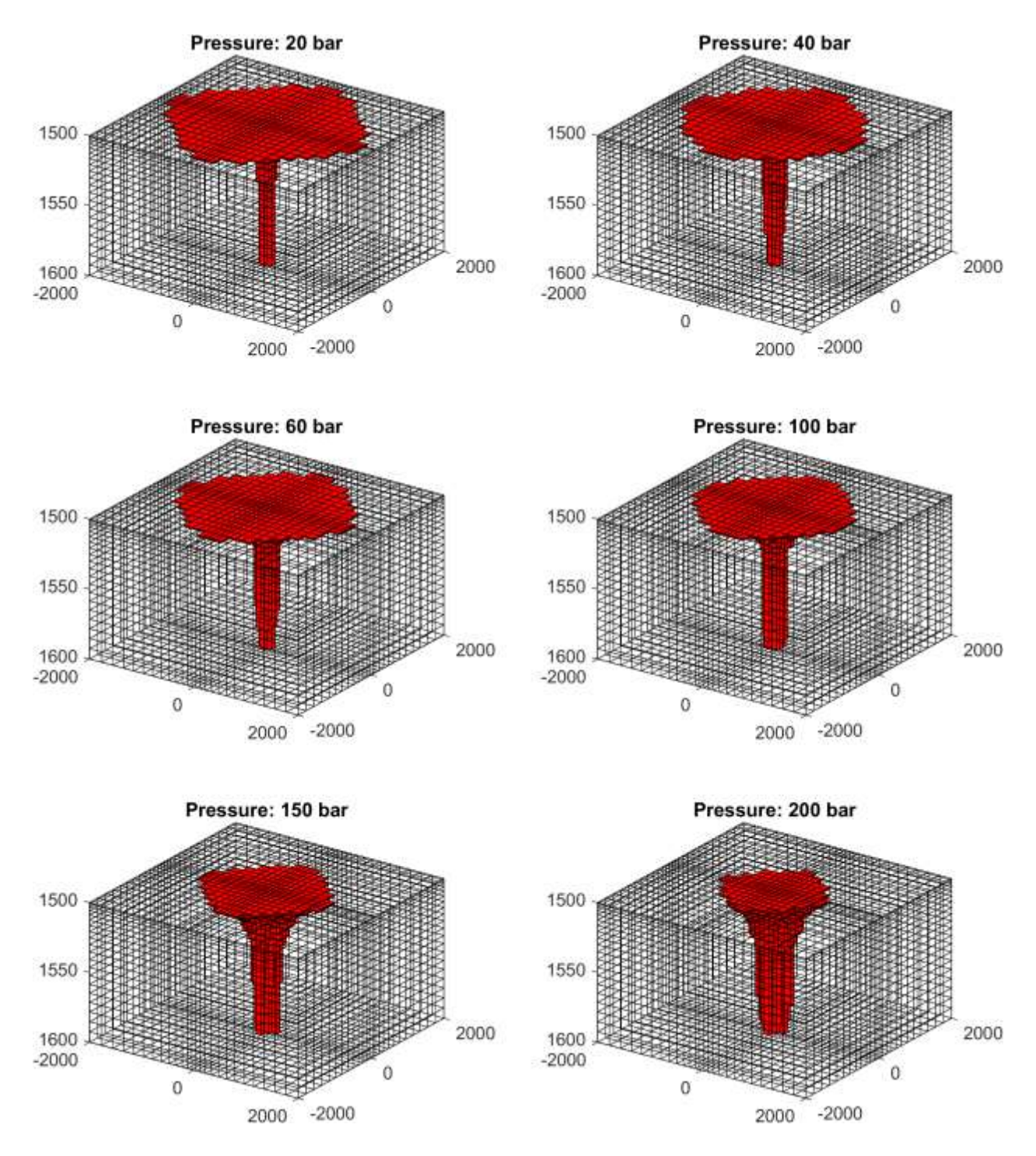


Figure 4 illustrates how pressure evolves within the reservoir over time, using a vertical slice through the domain at approximately  $x \approx 0$ . During the active injection phase, pressure builds up rapidly near the injection well as  $CO_2$  is introduced into the formation. This occurs because the injected  $CO_2$  displaces native fluids, reducing pore space availability and creating a localised pressure peak. The resulting pressure gradient drives the plume away from the well, aiding its buoyant migration through the reservoir. As the simulation transitions into the post-injection phase, this pattern begins to shift. With injection halted, the pressure near the well gradually declines as the  $CO_2$  redistributes throughout the formation and the system seeks to re-establish equilibrium. Some of the injected  $CO_2$  is absorbed into the reservoir fluids or becomes immobilised through trapping mechanisms, further reducing pressure in the plume's vicinity. Interestingly, the plume area eventually exhibits pressures lower than both the original baseline and the surrounding formation, highlighting the long-term impact of injection and the reservoir's dynamic adjustment.

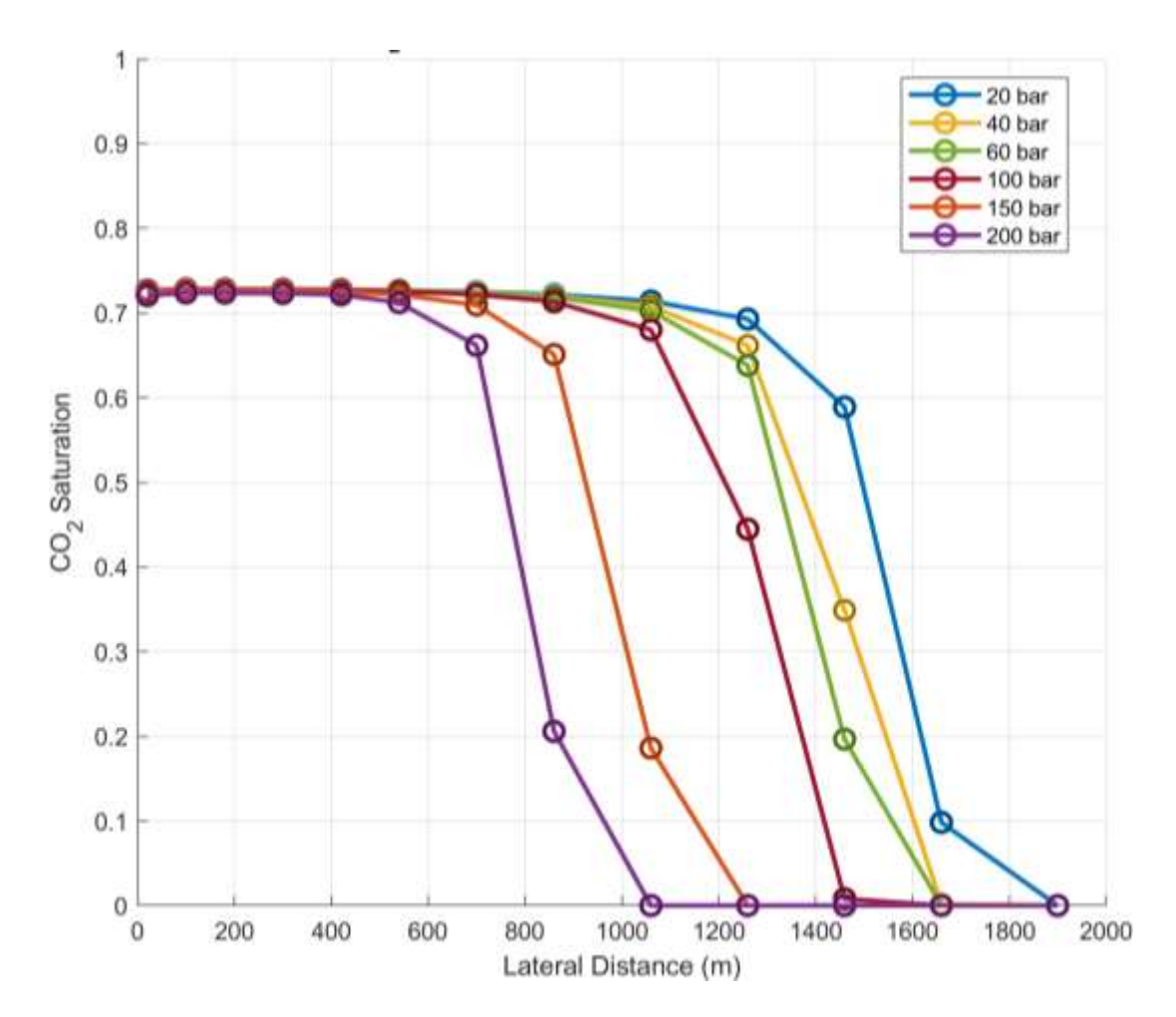
Figures 5 and 6 present the results of a sensitivity analysis assessing the effect of initial reservoir pressure on CO<sub>2</sub> plume migration. These figures collectively illustrate how varying the baseline pressure, from 20 to 200 bar, impacts the extent and distribution of injected CO<sub>2</sub> over time.

Figure 5 offers a visual comparison of CO<sub>2</sub> saturation at the final timestep (after two years of injection followed by two years of post-injection migration) for each pressure scenario. It shows that lower initial pressures result in significantly a broader plume spread. At 20 bar, for instance, the CO<sub>2</sub> plume expands laterally to over 1600 metres in radius. As the initial pressure increases, the extent of plume migration becomes progressively more constrained; at 200 bar, the plume reaches just over 800 metres. This inverse relationship between initial reservoir pressure and plume spread is clearly visible across the panels, suggesting that higher background pressure inhibits lateral plume migration by limiting the available pressure gradient that drives the flow. Figure 6 provides a complementary, quantitative view by showing the lateral distribution of CO<sub>2</sub> saturation in the uppermost reservoir layer for each pressure case. The curves indicate the maximum CO<sub>2</sub> saturation across lateral distances from the injection point, highlighting the same trend: wider and more pronounced plume footprints occur at lower pressures, while higher pressures lead to steeper declines in saturation with distance. It is noted that a fixed volumetric flow rate was used for all scenarios, which results in a higher mass of CO<sub>2</sub> being injected at elevated reservoir pressures due to increased CO<sub>2</sub> density. Consequently, the observed reduction in plume spread at higher pressures may be even more pronounced under a constant mass injection scenario.

Taken together, these figures highlight the importance of reservoir pressure as a controlling factor in the spatial evolution of injected  $CO_2$ . These findings have important implications for site selection and injection strategy. Lower initial reservoir pressures may enhance plume mobility and storage capacity by enabling broader  $CO_2$  distribution, potentially improving contact with trapping structures. However, they may also require more careful monitoring due to the increased spatial extent of  $CO_2$  migration. Conversely, higher-pressure reservoirs may offer more constrained plume behaviour, which could simplify containment but limit storage efficiency. These findings demonstrate that plume migration is increasingly constrained at higher reservoir pressures. This is due not only to reduced pressure gradients but also to the lower buoyancy of  $CO_2$  at elevated pressures, which limits its capacity to rise and spread laterally. As such, site selection must balance the containment benefits of higher-pressure formations against their reduced storage efficiency and plume mobility.



**Figure 5**: Sensitivity analysis of  $CO_2$  plume migration under varying initial reservoir pressures. The plots show  $CO_2$  saturation at the final timestep (2 years injection, 2 years post-injection) for pressures of 20, 40, 60, 100, 150, and 200 bar. Red regions indicate cells where  $CO_2$  saturation exceeds 0.05, highlighting the extent of plume migration at each pressure, illustrating the impact of pressure on  $CO_2$  distribution over time. The length scales are in meters.



**Figure 6**: Lateral spread of CO<sub>2</sub> saturation in the uppermost layer of the reservoir at the final timestep for varying initial pressures. The curves represent the maximum CO<sub>2</sub> saturation binned across lateral distance (0-2000 m) for pressures of 20, 40, 60, 100, 150, and 200 bar.

At temperatures of  $70^{\circ}$ C,  $CO_2$  transitions into the supercritical phase when the pressure exceeds 73.8 bar. Pressures above this threshold result in  $CO_2$  exhibiting liquid-like density and behaviour, which significantly influences migration and storage characteristics in depleted gas reservoirs. In the context of our sensitivity analysis, the pressure range of 20 bar to 200 bar spans the transition from a gaseous state at lower pressures to a dense, supercritical phase at higher pressures. This shift in  $CO_2$ 's phase has a direct impact on the extent and distribution of plume migration, with  $CO_2$  in the supercritical phase being denser and more mobile, thus altering the plume dynamics compared to its gaseous state.

Figure 7 illustrates the evolution of CO<sub>2</sub> trapping mechanisms within the reservoir over time during injection of a volume of CO<sub>2</sub> equivalent to 400 ktonnes. It provides a clear picture of how CO<sub>2</sub> is stored through different processes during injection and post-injection phases. The stacked area plot shows the distribution of CO<sub>2</sub> stored in structural, residual, and solubility trapping mechanisms, allowing for a quantitative comparison of these processes as they evolve over time.

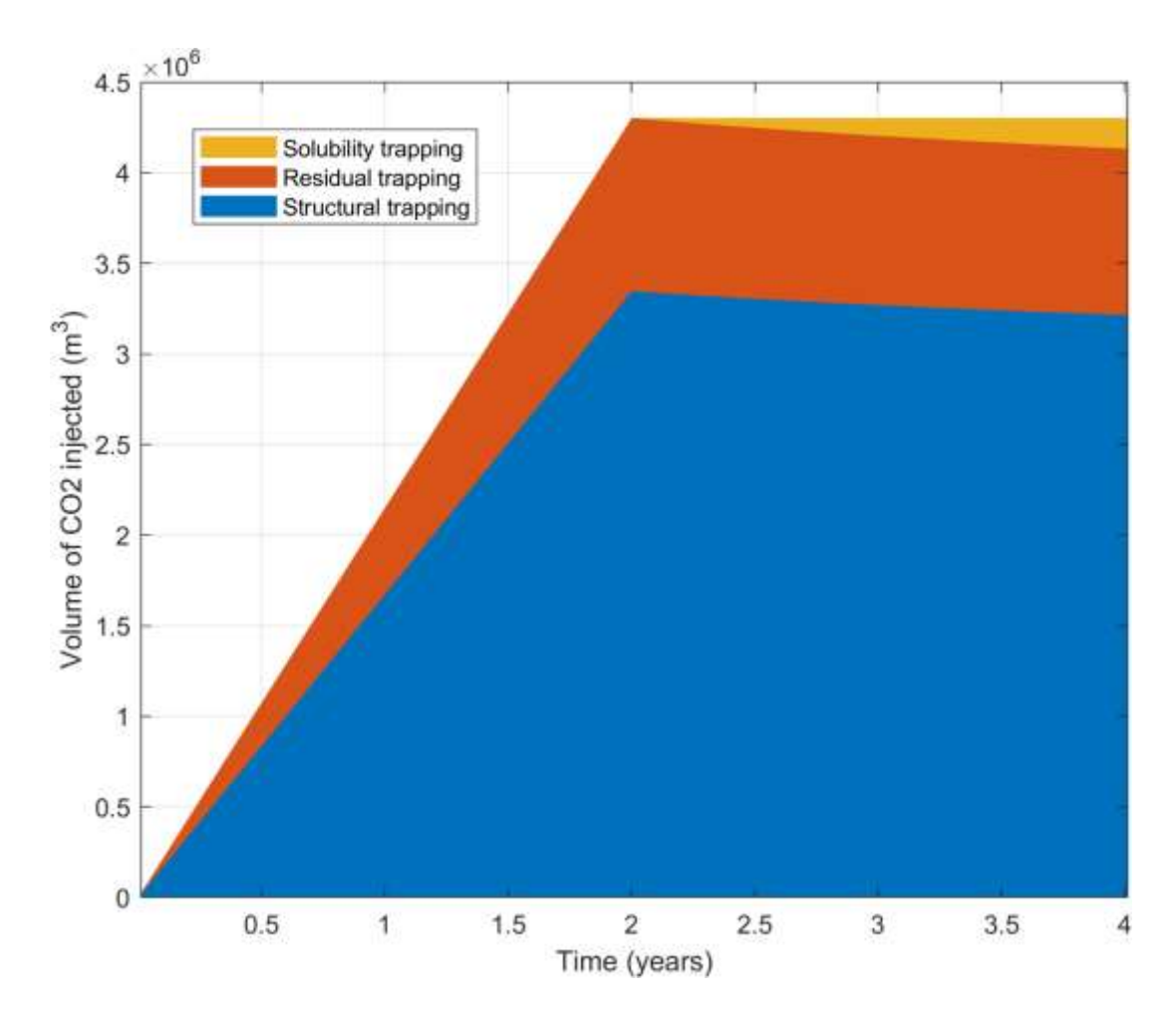


**Figure 7.** Evolution of CO<sub>2</sub> trapping mechanisms over time during geological storage, generated using the vertical equilibrium assumption. The stacked area plot illustrates the distribution of CO<sub>2</sub> (m<sup>3</sup>) among structural, residual, and solubility trapping mechanisms as a function of time (years).

During the injection phase, structural trapping is the dominant mechanism, as buoyant CO<sub>2</sub> migrates upwards and accumulates beneath the caprock. This is the initial and most immediate form of containment. As injection progresses, residual trapping begins to play a significant role, with CO<sub>2</sub> becoming immobilised in pore spaces due to capillary forces within the reservoir rock. After injection stops, the focus shifts to solubility trapping, where CO<sub>2</sub> gradually dissolves into the formation brine. Over time, the contribution of solubility trapping increases, while the role of structural trapping diminishes. This transition is typical in CO<sub>2</sub> storage scenarios, where structural trapping provides short-term containment, but solubility trapping becomes more significant over the long term, ensuring the stability and permanence of CO<sub>2</sub> storage.

#### Summary of basic simulation results

The basic simulations establish a foundational understanding of CO<sub>2</sub> injection dynamics in an idealised 3D reservoir model. These simulations show how the CO<sub>2</sub> plume evolves over time, initially spreading near the injection well and then expanding both laterally and vertically. Pressure



builds up in the reservoir during injection, especially close to the wellbore, as CO<sub>2</sub> displaces resident fluids.

Importantly, the simulations demonstrate the onset of key trapping mechanisms, of structural, residual, and solubility trapping, that contribute to long-term storage security. While mineral trapping was not explicitly modelled in this phase, the results underscore the fundamental physical processes governing plume migration and early CO<sub>2</sub> retention. These insights form a critical baseline for comparison with the more complex, realistic simulations that incorporate stream composition, reservoir heterogeneity, and geochemical interactions.

#### 7.2 Realistic simulation results

Building on the basic injection simulations, realistic numerical models were developed using the compositional module of MRST to assess CO<sub>2</sub> plume migration, pressure evolution, and geochemical interactions under more complex geological conditions. The models account for variable injection rates, CO<sub>2</sub> stream compositions, and formation heterogeneity to evaluate their impact on long-term storage security. A geochemical model may also be incorporated to assess mineral dissolution and precipitation effects.

# 7.2.1 Impact of injection stream composition and reservoir properties on CO<sub>2</sub> plume migration

Time evolution of the CO<sub>2</sub> Plume: Baseline with pure CO<sub>2</sub>

To establish a reference for plume development, a series of simulations were performed using pure  $CO_2$  injection. Figure 8 illustrates the time evolution of the  $CO_2$  plume over a 2-year period. At early timesteps (e.g., Day 33), the plume remains compact and is localised near the injection well. As time progresses (Days 146, 365, and 730), the plume expands, especially laterally upper more permeable part of the reservoir (Layer 2: Hardegsen High Perm). This baseline simulation provides essential insights into the intrinsic dynamics of plume migration under idealised conditions.



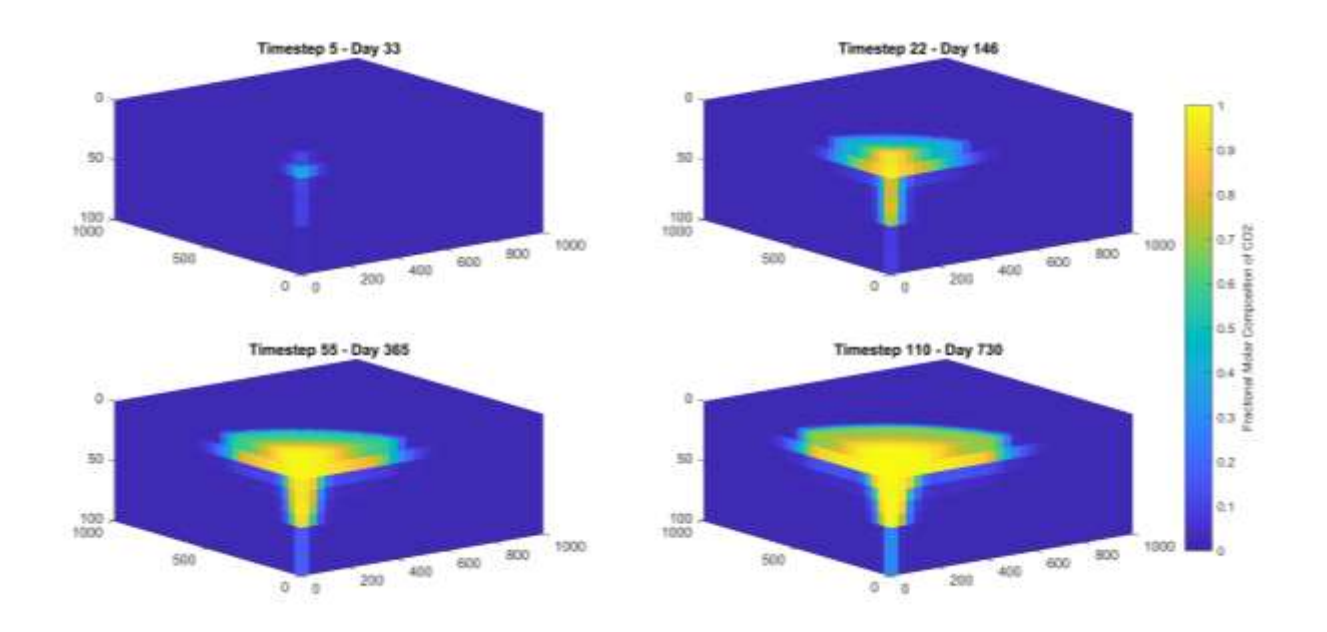


**Figure 8:** 3D plots showing the fractional molar composition of CO<sub>2</sub> at four selected timesteps (Days 33, 146, 365, and 730) during a 2-year simulation of pure CO<sub>2</sub> injection compositions. The colour-bar represents the CO<sub>2</sub> mole fraction.

#### Impact of CO<sub>2</sub>/N<sub>2</sub> stream composition on plume migration

Building on the pure  $CO_2$  baseline, additional simulations were performed by varying the proportions of  $CO_2$  and  $N_2$  in the injected stream. The objective was to assess how increasing  $N_2$  content, which reduces the overall density of the injected mixture, affects plume dynamics. The results as shown in Figure 9, indicate that as  $N_2$  content increases, the plume exhibits a broader lateral spread due to enhanced buoyancy effects. For instance, while the pure  $CO_2$  case shows a confined plume, mixtures with 95%, 80%, and 50%  $CO_2$  indicated a progressively wider plume migration by Day 730.

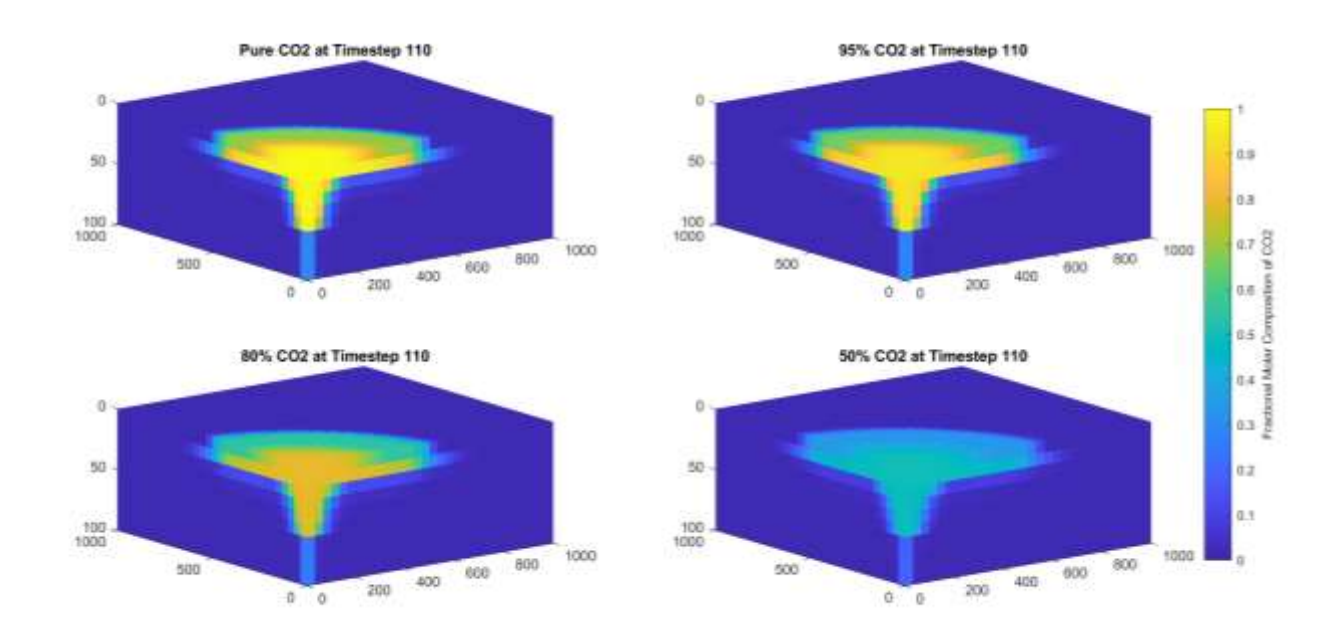


**Figure 9:** 3D plots comparing the fractional molar composition of  $CO_2$  at Day 730 for different  $CO_2/N_2$  mixtures (pure  $CO_2$ , 95%  $CO_2$ , 80%  $CO_2$ , and 50%  $CO_2$ ). The plots highlight the influence of  $N_2$  dilution on plume lateral extent.

#### Sensitivity analysis on permeability and porosity

A series of simulations were performed to assess the impact of variations in reservoir porosity and permeability on  $CO_2$  plume migration. The sensitivity analysis focused on incremental increases of 10%, 20%, 30%, and 40% above the base-case values of permeability and porosity, with the aim of quantifying how these changes influence the lateral spread and retention of the  $CO_2$  plume. The results are shown in Figure 10.

#### Key observations are:

- Porosity effects: Increasing porosity enhances the storage capacity of the reservoir by expanding the available pore space. As porosity increases, a greater fraction of the injected CO<sub>2</sub> is retained within the rock matrix, resulting in a reduced lateral migration of the plume.
- **Permeability effects:** Within the tested range, variations in permeability exert a less pronounced effect on plume migration compared to porosity. Although higher permeability facilitates fluid movement, its impact on the lateral spread of the plume is minimal unless the change is substantial.

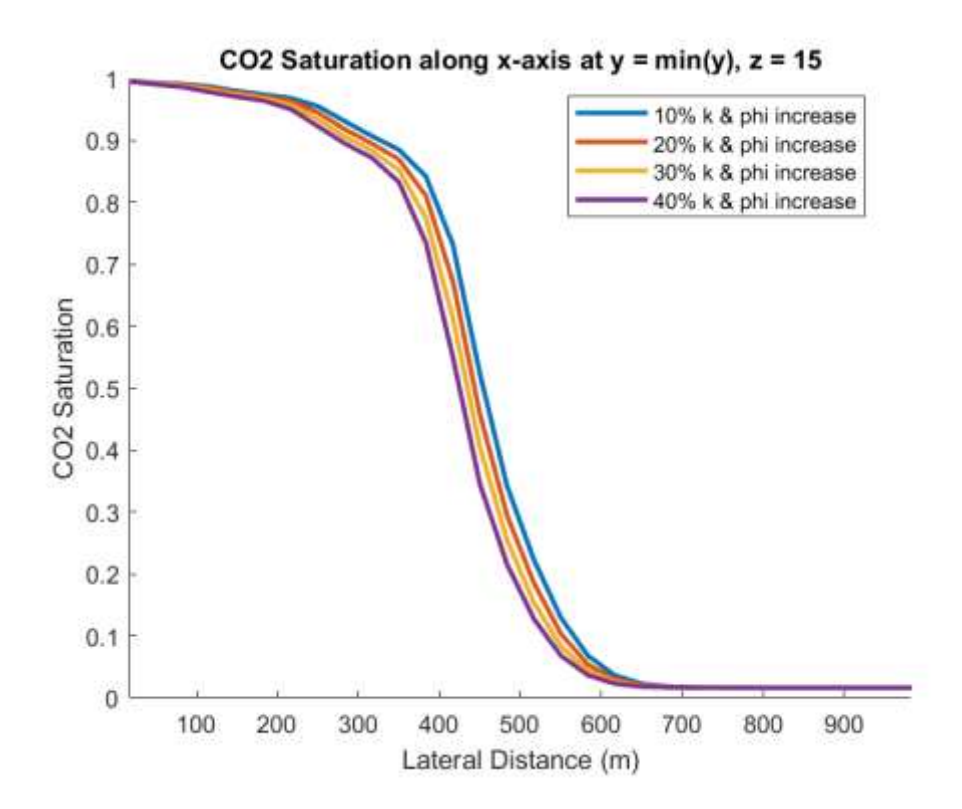


**Figure 10:** Illustration of the lateral  $CO_2$  saturation profile for different permeability and porosity values (10%, 20%, 30%, and 40% increases relative to the base case). The results demonstrate that increased porosity leads to a reduction in the lateral spread of the  $CO_2$  plume, indicating improved  $CO_2$  retention within the reservoir.

#### 7.2.2 Impact of variable injection flow rates

Injection strategy plays a key role in determining both the pressure evolution within the reservoir and the mechanical stability of the injection zone. To investigate this, simulations were conducted to compare the effects of two different injection profiles: a constant high-rate injection versus a stepwise, staged increase in flow rate. These scenarios help illustrate how flow rate management can influence near-well pressure dynamics and overall injectivity.

In the continuous injection scenario (Figure 10), the reservoir experiences a pronounced pressure spike early on because the injected  $CO_2$  must initially displace brine, which offers higher flow resistance. During this phase, the region around the well is predominantly brine-saturated, so introducing  $CO_2$  at a constant high rate forces a rapid buildup of pressure in the monitoring cell. As injection proceeds, however, more of the near-well region transitions from brine to  $CO_2$ . Because  $CO_2$  is generally less viscous and easier to inject than brine, pressure eventually begins to decline or at least stops climbing further. Over time, natural flow and redistribution processes within the reservoir also help to move  $CO_2$  away from the wellbore, further mitigating the pressure peak.



In contrast, the stepwise injection strategy gradually ramps up the injection rate in stages (as shown in Figure 11), reducing the initial pressure spike. Each stage allows the reservoir to partially equilibrate, so when the rate increases again, the near-well region is already more CO2-rich and less brine-saturated than it was at the outset. As a result, the maximum pressure in the monitoring cell during the early phase of injection is lower than in the continuous scenario, even though the total volume of CO² injected over the same time period is the same. This more controlled approach can be especially valuable in reservoirs where over-pressurisation poses a risk to well integrity, as it minimises abrupt pressure surges while still achieving the desired injection targets.

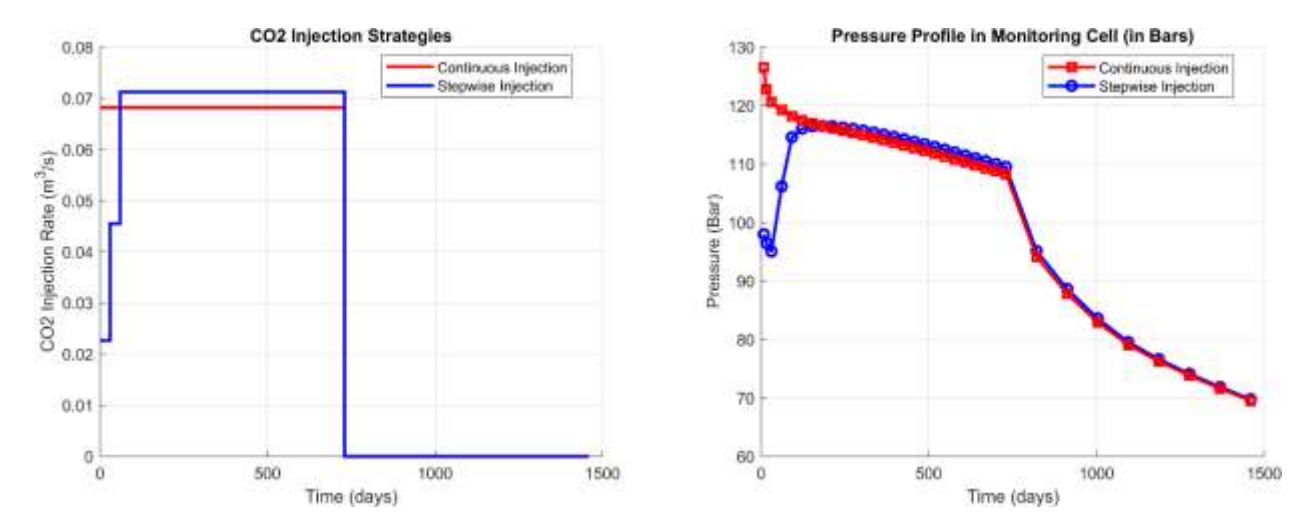


**Figure 11.** CO<sub>2</sub> injection strategies and pressure profile in the monitoring cell. The plot on the left shows continuous and stepwise CO<sub>2</sub> injection rates over a 4-year period, with the injection rates dropping to zero after 2 years, while the stepwise injection follows a multi-stage pattern. The plot on the right displays the corresponding pressure profile (in bar) in the monitoring cell above the injection point, showing the response to both injection strategies over time.

#### 7.2.3 Geochemical interactions

To evaluate the long-term security of  $CO_2$  storage, it is essential to understand how injected  $CO_2$  interacts with the geochemical environment of the reservoir. In particular, mineral-fluid reactions can influence porosity, permeability, and overall storage integrity over time. The geochemical module within the MRST framework was used to simulate these interactions, offering insight into the spatial and temporal evolution of aqueous species and their equilibria with mineral phases. By capturing dissolution, precipitation, and acid-base reactions, the model helps to illuminate how  $CO_2$  injection perturbs chemical equilibria and what implications these have for mineral stability and fluid composition throughout the domain.

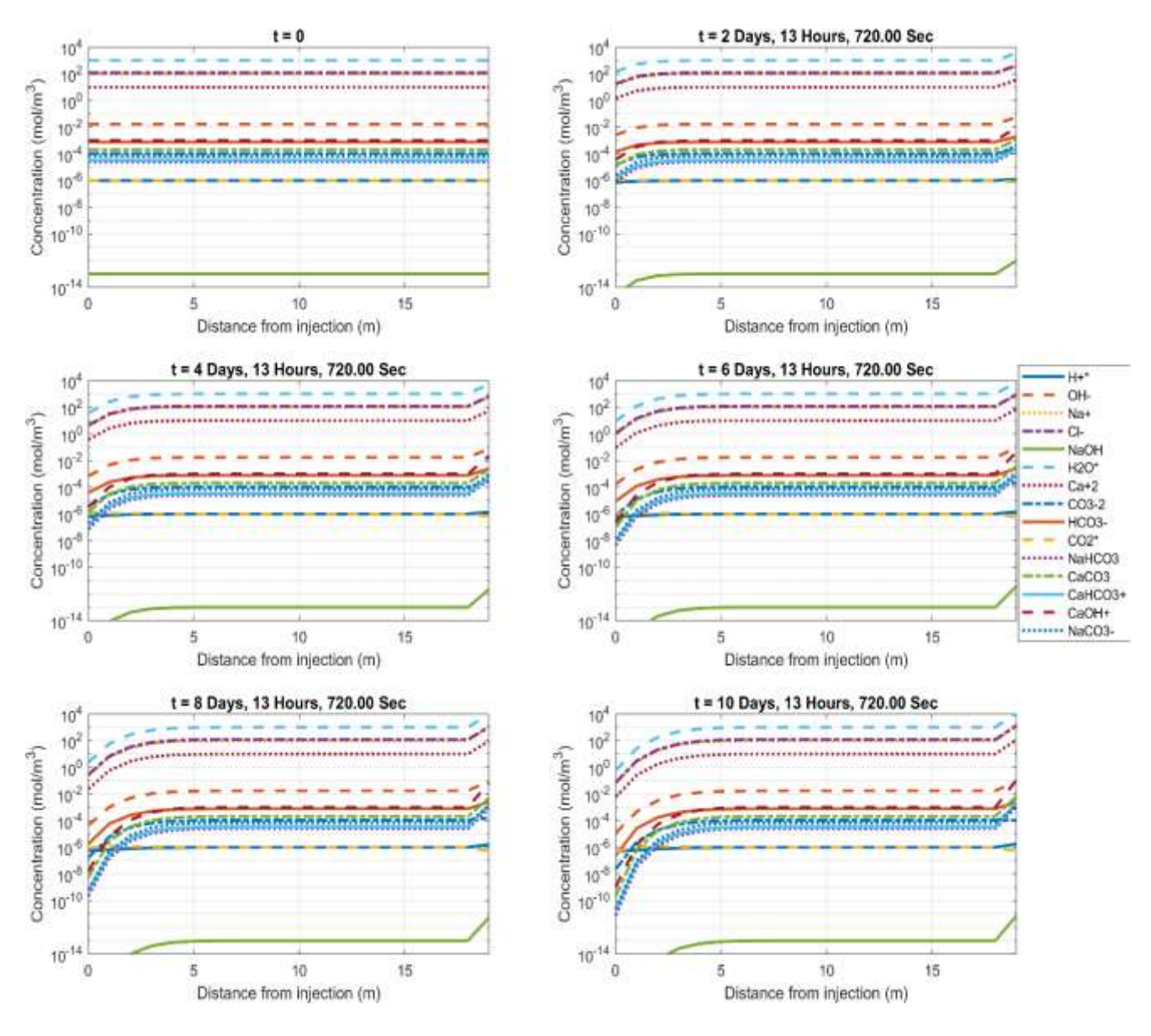


**Figure 12.** Evolution of chemical species concentrations along the bottom row of a 20-cell domain as a function of distance from the injection point, at selected simulation time steps. Concentrations (in mol/m³, displayed on a logarithmic scale) of 15 tracked species are shown, illustrating the reactive transport and evolving chemistry as a low-salinity fluid is injected into a high-salinity reservoir.

The line plots in Figure 12 illustrate the spatial and temporal evolution of various aqueous chemical species in a 2D reservoir domain subject to  $CO_2$  injection. Each subplot corresponds to a specific time step (0, 2, 4, 6, 8, and 10 days), with the x-axis representing the distance from the injection point to the producer (0 to 20 units) and the y-axis depicting concentration on a logarithmic scale from approximately  $10^3$  to  $10^{-13}$  mol/m³.



At time zero, all species are evenly distributed across the domain, as expected from the uniform initial conditions. Over time, significant geochemical changes emerge near the injection point due to the perturbation caused by the introduction of  $CO_2$ -rich brine. Most species show a marked decline in concentration in this region, with the effect intensifying at later time steps, reflecting increasing dissolution, speciation, or buffering reactions driven by acidification. Exceptions include  $H^+$  and  $CO_2(aq)$ . These two species exhibit only subtle declines near the injection point, with  $H^+$  decreasing more gradually than  $CO_2(aq)$ , suggesting limited chemical reactivity or early-stage buffering effects in the immediate vicinity. Their subdued dynamics suggest that  $CO_2$  dissolution and pH changes are the primary driving forces, but equilibrium is quickly established for these two species compared to others.

The absence of an increase in H<sup>+</sup> concentration despite CO<sub>2</sub> injection indicates strong buffering within the system. As CO<sub>2</sub> dissolution would normally drive acidification, rapid reaction with carbonate species mitigates any substantial rise in free protons. In particular, carbonate equilibria, especially the dissolution of CaCO<sub>3</sub>(s), even though it is not explicitly tracked in the simulation, play a crucial role by converting H<sup>+</sup> into bicarbonate (HCO<sub>3</sub><sup>-</sup>) or other associated species. Consequently, the rapid adjustment of these reactions maintains a nearly constant H<sup>+</sup> level, with only subtle declines observed near the injection point, indicating the system's inherent resistance to pH changes during early CO<sub>2</sub> injection stages.

In the central region of the domain, concentrations remain close to initial values throughout, reflecting a chemical 'buffer zone' largely unaffected by the  $CO_2$  front migration within the 10-day simulation window. Near the producer well, several species exhibit a slight uptick in concentration at the final cell (a sharp, localised increase rather than a gradient), which may result from mild accumulation or back-diffusion effects. This subtle buildup is less pronounced than the depletion seen near the injector and is species-dependent: it's more visible in ions such as  $Na^+$ ,  $Cl^-$ , and  $HCO_3^-$ , while  $CO_3^{2-}$  and  $CO_2(aq)$  show a level profile and continued decline, respectively, possibly due to precipitation or ongoing reactivity.

In summary, the chemical profiles reveal a clear asymmetry in system response: intense reactivity and depletion near the injector, stability in the mid-domain, and minor enrichment near the producer. These trends highlight the interplay of advection, dispersion, and chemical kinetics particularly the sensitivity of carbonate equilibria and ion exchange to acidified CO<sub>2</sub> front propagation.



#### 8. Discussion and geotechnical evaluation

In this final section, we draw together the pressure, saturation, and geochemical outputs from our basic and realistic simulations to derive first-order geotechnical insights into CO<sub>2</sub> storage stability. Rather than attempting a full mechanical or fracture-slip analysis, we have stayed within the bounds of our existing MRST results; namely, 3D pressure fields, CO<sub>2</sub>-saturation maps, and reactive-transport species profiles, and interpreted them in terms of seal integrity, plume confinement, and mineral feedback over reservoir-relevant timescales.

In the homogeneous injection-strategy runs, we extracted vertical slices of the pressure field at Days 33, 146, 365, and 730, alongside the time series recorded in our single monitoring cell immediately above the injector (Figure 10). In the continuous injection case, a sharp pressure spike early on reflects the need to displace brine within the near-well region; as more CO<sub>2</sub> occupies pore space, injection becomes easier and the pressure plateau or even declines slightly. The stepwise ramp-up schedule, by contrast, showed a more gradual pressure increase: each new rate step begins from a higher CO<sub>2</sub> saturation and hence lower flow resistance, capping the peak pressure at each stage.

Although we have not imposed a specific caprock fracture threshold in our analysis, these curves nonetheless reveal the time windows, particularly the first two months, when over pressurisation is most pronounced and well integrity would need the closest monitoring. Moreover, the pressure dissipation during the shut-in period (post-Day 730) indicates how quickly the system returns toward equilibrium, providing an estimate of the timescales over which elevated pressures persist.

Overlaying CO<sub>2</sub>-saturation contours on 3D, plan-views, and cross-sections (Figures 1-3 and 8) allows us to assess lateral and vertical plume confinement relative to the caprock interval. In the P18-6 analogue, even under maximum injection rates, the plume remains confined to the reservoir extent at recorded timesteps; lateral growth begins to taper after roughly one year, consistent with the pressure gradient decline noted above.

In our homogeneous grid, the residual "wake" or footprint of trapped  $CO_2$  visible as light-blue zones in Figure 2, highlights regions where capillary and solubility trapping immobilise  $CO_2$  behind the leading plume front. The extent and intensity of this residual zone provide a proxy for early-stage storage security: the more substantial and continuous the residual saturation, the less mobile  $CO_2$  remains once buoyant forces abate.

Within the  $20 \times 1 \times 1$  reactive slice, we tracked 15 (amongst 17 simulated) aqueous and mineral species over ten days of injection (Figure 11). Although full reactive equilibrium takes longer, the concentration profiles reveal clear geochemical gradients: near the injector, rapid acidification drives significant depletion of carbonate species and cations, indicating that calcite dissolution would predominate in this zone. Further downstream, species concentrations return toward their initial levels, suggesting that re-precipitation or buffering reactions would begin to re-stabilise mineral phases.

These spatial patterns of strong dissolution closest to the well and nascent precipitation farther away imply that injectivity may improve in the early stage (as pore volumes temporarily increase)



but could gradually decline where secondary minerals form. Mapping these zones thus provides a qualitative forecast of where permeability enhancement or reduction might occur.

Taken together, our diagnostics of pressure curves, plume-extent timelines, and geochemical zoning form a reproducible framework for preliminary geotechnical evaluation. Key takeaways include:

- **Pressure management** is critical during the first months of injection; ramped injection can substantially mitigate peak pressures.
- **Plume confinement** under our P18-6 analogue remains well within reservoir extents, even for high-rate scenarios.
- **Residual trapping** footprints develop rapidly and offer early security against CO<sub>2</sub> remobilisation.
- **Mineral feedbacks** may enhance injectivity near the well but could contribute to porespace reduction downstream over longer timescales.

Although our approach stops short of explicit geomechanical or fracture modelling, it leverages existing MRST outputs to highlight when and where overpressure, plume migration, and geochemical alteration intersect to influence storage security. These insights could form the basis for targeted monitoring plans, such as pressure monitoring and sampling wells, and for the future computation work, which could incorporate coupled geomechanical simulations and long-term reactive transport to validate and extend these evaluations.



#### 9. Summary and conclusions

In this work, we have taken a systematic approach to understanding CO<sub>2</sub> storage in depleted gas reservoirs, starting from method development and ending with first-order geotechnical insights. We began our investigation with a series of controlled, homogeneous reservoir experiments using MRST's CO<sub>2</sub>-lab module. In these basic simulations, pure CO<sub>2</sub> was injected at a constant volumetric rate into a three-dimensional grid of uniform porosity and permeability. By varying only the background pressure while holding all other parameters fixed, we observed the classic buoyant rise and lateral spread of the CO<sub>2</sub> plume, the sharp pressure spike near the injector and its gradual dissipation, and the sequential dominance of structural, residual, and solubility trapping over the course of two years of injection and two years of shut-in. These foundational runs established how initial reservoir conditions alone dictate plume footprint, driving forces for migration, and the onset of key trapping mechanisms.

Building on the basic simulations, we introduced geological complexity and operational variation in a five-layer P18-6 analogue. Field-derived porosities and permeabilities gave rise to high-permeability channels that preferentially guided the plume, while lower-permeability horizons acted as containment barriers. We then explored the effect of stream composition by adding N<sub>2</sub> revealing that dilutions broaden plume spread via reduced density. We also tested both constant-rate and stepwise ramp-up injection schedules. The staged approach noticeably reduced early pressure peaks by leveraging the progressively easier injectivity of a CO<sub>2</sub>-rich near-well region.

Next, we brought MRST's geochemical toolbox to bear on a simplified 20×1×1 reactive slice. Here, rapid acidification and calcite dissolution dominated the region immediately adjacent to the injector, temporarily opening up pore space, while downstream zones trended back toward equilibrium through nascent mineral precipitation. These chemically active fronts mapped out where injectivity might initially improve and where pore-space reduction could set in over longer timescales.

Rather than pursuing a full geomechanical treatment, the extraction of three-dimensional pressure fields, CO<sub>2</sub>-saturation maps, and species-concentration profiles enabled the derivation of first-order geotechnical insights. The most intense overpressure occurs in the earliest weeks of injection, highlighting the critical window for well-integrity monitoring, while the residual "wake" in saturation slices provides an early indicator of immobilised CO<sub>2</sub>. Our geochemical zoning, meanwhile, qualitatively forecasts where permeability enhancements and reductions may emerge, steering expectations for injectivity longevity and storage security.

Taken together, this tiered workflow, from homogeneous benchmarks, through realistic heterogeneity and compositional tests, to geochemical profiling, forms a reproducible path from raw simulation data to practical, field-relevant insights. Key conclusions are:

- **Pressure management:** Staged, ramp-up injection can substantially reduce early pressure spikes, focusing operational vigilance on the first few months of injection.
- Plume confinement: Natural heterogeneity both guides and bounds the plume, confirming that, under our P18-6 analogue conditions, lateral growth begins to taper after roughly one year.



- **Early trapping indicators:** Residual CO<sub>2</sub> zones with low saturation form quickly near the injector, providing early evidence of effective residual and solubility trapping mechanisms during the injection phase and post-injection migration.
- **Mineral feedbacks:** Geochemical fronts delineate zones of early injectivity gains (via dissolution) and later injectivity losses (via precipitation), helping anticipate potential well maintenance needs and changes in storage performance over time.

Looking forward, integrating these diagnostics with explicit geomechanical simulations, switching to mass-based injection controls, accounting for thermal effects (Joule–Thomson cooling/heating), and extending reactive-transport horizons will be critical steps toward fully validated, field-ready CO<sub>2</sub> storage strategies.



#### 10. Bibliography / References

- [1] E. Commission, "Progress made in cutting emissions," Climate action, 2019. [Online]. Available: https://ec.europa.eu/clima/eu-action/climate-strategies-targets/progress-made-cutting-emissions\_en. [Accessed 29 March 2025].
- [2] B. Metz, O. D. Davidson, H. de Coninck, M. Loos and L. Meyer, "IPPC, Intergovernmental Panel on Climate Change: Special Report on Carbon Dioxide Capture and Storage.," in *IPPC Special Report*, Cambridge, Cambridge University Press, 2005, pp. 1-402.
- [3] IEA (International Energy Agency), "Exploring Clean Energy Pathways," IEA, Paris, 2019.
- [4] IEAGHG (IEA Greenhouse Gas R&D Programme), "Managing the Transition of Depleted Oil and Gas Field to CO<sub>2</sub> Storage: Technical Report 2024-05," IEA Greenhouse Gas R&D Programme, Cheltenham, 2024.
- [5] M. Hedayati, A. Wigston, J. L. Wolf, D. Rebscher and A. Niemi, "Impacts of SO<sub>2</sub> gas impurity within a CO<sub>2</sub> stream on reservoir rock of a CCS pilot site: Experimental and modelling approach," *International Journal of Greenhouse Gas Control* 70, vol. 70, pp. 32-44, 2018.
- [6] K.-A. Lie, An Introduction to Reservoir Simulation Using MATLAB/GNU Octave: User Guide for the MATLAB Reservoir Simulation Toolbox (MRST), Cambridge: Cambridge University Press, 2019.
- [7] K. -A. Lie and O. Møyner, Advanced Modeling with the MATLAB Reservoir Simulation Toolbox (MRST), Cambridge: Cambridge University Press, 2021.
- [8] A. Satter and G. M Iqbal, "3 Reservoir rock properties," in *Reservoir Engineering: The Fundamentals, Simulation, and Management of Conventional and Unconventional Recoveries*, Gulf Professional Publishing, 2016, pp. 29-79.
- [9] F. Neele, T. Wildenborg, K. Geel, D. Loeve, L. Peters, S. Kahrobaei, T. Candela, M. Koenen, P. Hopmans, K. van der Valk, B. Orlic and V. Vandeweijer, "CO₂ Storage Fea-sibility in the P18-6 Depleted Gas Field. TNO 2019 R11212," TNO, Utrecht, 2020.
- [10] B. Mallison, M. Gerritson, K. Jessen and F. M. J. Orr, "High Order Upwind Methods for Two-phase, Multicomponent Flow," in *SPE 79691*, Texas, 2003.